Earth and Planetary Science Letters 283 (2009) 14–23

Contents lists available at ScienceDirect

Earth and Planetary Science Letters

journal homepage: www.elsevier.com/locate/epsl

Stacking paleointensity and oxygen isotope data for the last 1.5 Myr (PISO-1500)

J.E.T. Channell *, C. Xuan, D.A. Hodell [1]

Department of Geological Sciences, University of Florida, 241 Williamson Hall, POB 112120, Gainesville, FL 32611, USA

ARTICLE INFO

Article history:
Received 26 September 2008
Received in revised form 2 February 2009
Accepted 5 March 2009
Available online 5 May 2009

Editor: P. DeMenocal

Keywords:
relative paleointensity stack
oxygen isotope stack
virtual axial dipole moment

ABSTRACT

Coupled relative geomagnetic paleointensity (RPI) and oxygen isotope records are used to construct RPI and oxygen isotope stacks for the last 1.5 Myr. The coupled correlations are accomplished using the Match algorithm (Lisiecki, L.E., and Lisiecki, P.A., 2002. Application of dynamic programming to the correlation of paleoclimate records. Paleoceanography, 17: 1049, doi:10.1029/2001PA000733) to simultaneously correlate isotope and RPI records. The simultaneous match reduces the degree of freedom associated with correlations using RPI or oxygen isotope records alone. The overall compatibility of RPI and oxygen isotopes indicates a dominant global (but independent) component in both signals. The local wavelet power spectrum (LWPS) for the RPI stack indicates little significant orbital power, although the accompanying oxygen isotope stack has all the LWPS characteristics expected of a high-resolution oxygen isotope record containing orbital frequencies. The PISO-1500 stack represents a new stratigraphic template that can be used to correlate among marine sediment records and link them to polar ice cores via variations in cosmogenic nuclide production. Scaling the stack to values for virtual axial dipole moment (VADM) indicate maxima at ~15×10^{22} Am^2 and minima that imply a threshold of ~2.5×10^{22} Am^2 below which values are associated with either polarity reversals or magnetic excursions.

1. Introduction

The quest for improved stratigraphic correlation remains one of the great challenges in paleoceanography. Since Shackleton (1967) made the case for oxygen isotopic data as a monitor of global ice volume, benthic $\delta^{18}O$ has been the hallmark of marine stratigraphy, however, oxygen isotope changes in seawater are not globally synchronous on (millennial) timescales associated with the mixing time of the oceans (e.g. Skinner and Shackleton, 2005). Although oceanic mean $\delta^{18}O$ will reflect global ice volume change over multi-millennia, an individual benthic $\delta^{18}O$ record will reflect both global glacio-eustatic and local hydrographic signals (temperature and deep-water $\delta^{18}O$) to varying degrees (Skinner and Shackleton, 2006).

There would be great advantage in coupling oxygen isotopes with an independent stratigraphic tool that is global in nature and devoid of environmental influences. Traditional magnetic stratigraphy, the observation of polarity zones in sedimentary sections, has become the backbone of geologic timescales partly because polarity reversal is a geophysical phenomenon attributable to the main dipole field, and therefore provides global timelines for precise correlation at the time of reversal. Accumulation of relative paleointensity (RPI) data in the last 10 yr holds the promise of stratigraphic correlation within polarity chrons, possibly at millennial scale. The association of some RPI minima with brief magnetic excursions means that there is a manifestation of RPI stratigraphy in the paleomagnetic directional record.

A first step in the utilization of paleointensity records in stratigraphy is the development of a calibrated template. As for benthic oxygen isotopes, a template based on multiple records rather than an individual record, has the advantage of increasing the signal to noise ratio in that local or regional change recorded by individual records may be averaged out by the stacking process. The disadvantage of stacks, on the other hand, is that the stacking process inevitably reduces the resolution of the output, compared to the input of individual records. Several paleointensity stacks have been produced in the last 10 yr including Sint-800 and Sint-2000 (Guyodo and Valet, 1999; Valet et al., 2005) covering the last 800 and 2000 kyr, respectively. For the last 75 kyr, regional stacks for the North Atlantic (NAPIS) (Laj et al., 2000) and South Atlantic (SAPIS) (Stoner et al., 2002), and a global stack (GLOPIS) (Laj et al., 2004), have been generated. The EPAPIS stack from the western equatorial Pacific covers the 0.75–3.0 Ma interval (Yamazaki and Oda, 2005). Here we present a stack that differs from earlier stacks in that the stacking process is conducted simultaneously on both oxygen isotope and RPI data. The stack includes, therefore, only RPI records that have accompanying oxygen isotope records. Most of the coupled RPI-isotope records included here (Table 1) have not been included in previously derived RPI stacks, at least not in their entirety.

* Corresponding author. Tel.: +1 352 392 3658; fax: +1 352 392 9294.
E-mail address: jetc@geology.ufl.edu (J.E.T. Channell).
[1] Current address: Godwin Laboratory for Paleoclimate Research, Department of Earth Sciences, University of Cambridge, Downing Street, Cambridge, CB2 3EQ, (UK).

0012-821X/$ – see front matter © 2009 Elsevier B.V. All rights reserved.
doi:10.1016/j.epsl.2009.03.012

Table 1
Records used in the construction of the PISO-1500 stacks.

Record	Loc.	Lat.	Long.	WD (m)	Length (m)	Age range (ka)	Ave. sedimentation rate (cm/ky)	Iso	Ref.
IODP U1308	N.Atl.	49°53'N	24°14'	3871	109	5–1500	7.3	B	1
ODP 983	N.Atl.	60°24'N	23°38'W	1983	199	5–1500	13.3	B	2
ODP 984	N.Atl	61°26'N	24°05'W	1648	183	5–1500	12.2	B	3
ODP 919	N. Atl	62°40'N	37°28'W	2088	83	9–540	15.4	P	4
ODP 980	N.Atl	55°29'N	14°42'W	2168	116	20–1300	8.9	B	5
PS 2644	N.Atl	67°52'N	21°46'W	777	9.2	12–76	12.1	P	6
MD95-2024	N.Atl	50°12'N	45°41'W	3448	27.3	5–110	24.8	P	7
MD99-2227	N.Atl	58°07'N	48°13'W	3460	43	1–430	10.0	P	8
MD95-2039	N.Atl	40°35'N	10°21'W	3381	35.7	30–317	11.3	B	9
ODP 1089	S.Atl	40°56'S	9°54'E	4624	90	20–580	15.5	B	10
MD97-2140	W.Pac	2°3'N	141°46'E	2547	12.5	560–1300	1.7	B	11
MD97-2143	W.Pac	15°52'N	124°39'E	2989	23.3	7–1500	1.6	B	12
Somali	Ind	0°1'S	46°2'E	4020	6.8	12–140	4.9	Bulk	13

The "Iso" column refers to the planktic (P), benthic (B) or "bulk" source of oxygen isotope data.
References ("Ref"): (1) Channell et al., 2008; Hodell et al., 2008 (2) Channell et al., 1997, 2002; Channell, 1999; Channell and Kleiven, 2000 (3) Channell, 1999; Channell et al., 2002, 1997 (4) Channell, 2006 (5) Channell and Raymo, 2003 (6) Laj et al., 2000; Voelker et al., 1998 (7) Stoner et al., 2000 (8) Evans et al., 2007 (9) Thouveny et al., 2004; Thomson et al., 1999 (10) Stoner et al., 2003 (11) Carcaillet et al., 2003, 2004; De Garidel-Thoron et al., 2005 (12) Horng et al., 2002, 2003 (13) Meynadier et al., 1992.

The new RPI/isotope stack (named PISO-1500) provides a new template for correlation and calibration of RPI and isotope records. The fidelity of the accompanying oxygen isotope stack can be tested by comparison with a widely-used calibrated oxygen isotope stack (Lisiecki and Raymo, 2005). This exercise can gauge the level of consistency of the two stratigraphies, and possibly determine whether the RPI correlations enhance isotopic correlations when the records are used in tandem.

2. The Match and the stack

The potential of RPI for high-resolution correlation stems from the high rate of change of the Earth's dipole field intensity, that has decreased by ~5% over the last 100 yr in the historical record, and by ~20% over the last 1000 yr in the archaeological record (Korte and Constable, 2005; Valet et al., 2008). In comparison, the rate of change of global ice volume (the basis for benthic δ^{18}O stratigraphy) tends to be greatest at glacial terminations but relatively slow otherwise. Benthic δ^{18}O shows comparatively little variability during marine isotopic stage (MIS) 2–4 (20–80 ka) in contrast to RPI variations in this interval. Previous RPI stacks involve some form of visual matching of features in RPI records that can be arbitrary, and poorly constrained. To make signal correlation more objective, we use the Match protocol (Lisiecki and Lisiecki, 2002) that utilizes dynamic programming to find the optimal fit between record pairs. The method was used by Lisiecki and Raymo (2005) to construct their benthic oxygen isotope stack (LR04). We apply the protocol simultaneously to isotope and RPI records for 12 published records (Table 1, Fig. 1) to optimize their fit to IODP Site U1308 records. We use Site U1308 as the reference record for the stack, because the site has high-resolution benthic isotope and RPI data for the entire 1.5 Myr interval (Channell et al., 2008; Hodell et al., 2008). The age model for Site U1308 was constructed by fit of the benthic oxygen isotope record to LR04 (Hodell et al., 2008). At ODP Sites 983 and 984 (Fig. 1, Table 1), the RPI records have higher resolution than the accompanying isotope records which are limited by paucity of foraminifera prior to 1.1 Ma (Channell, 1999; Channell et al., 2002, 1997; Channell and Kleiven, 2000). The only other record that spans the full 1.5 Myr interval is Core MD97-2143 (Horng et al., 2002, 2003); however, this record has lower mean sedimentation rate, than ODP Sites 983/984, by almost an order of magnitude (Table 1). Other records included in the stack cover parts of the 1.5 Myr interval: ODP Site 980 (Channell and Raymo, 2003) extends back to 1.3 Ma, ODP Site 919 (Channell, 2006) extends back to 540 ka, ODP Site 1089 (Stoner et al., 2003) extends back to 580 ka, MD99-2227

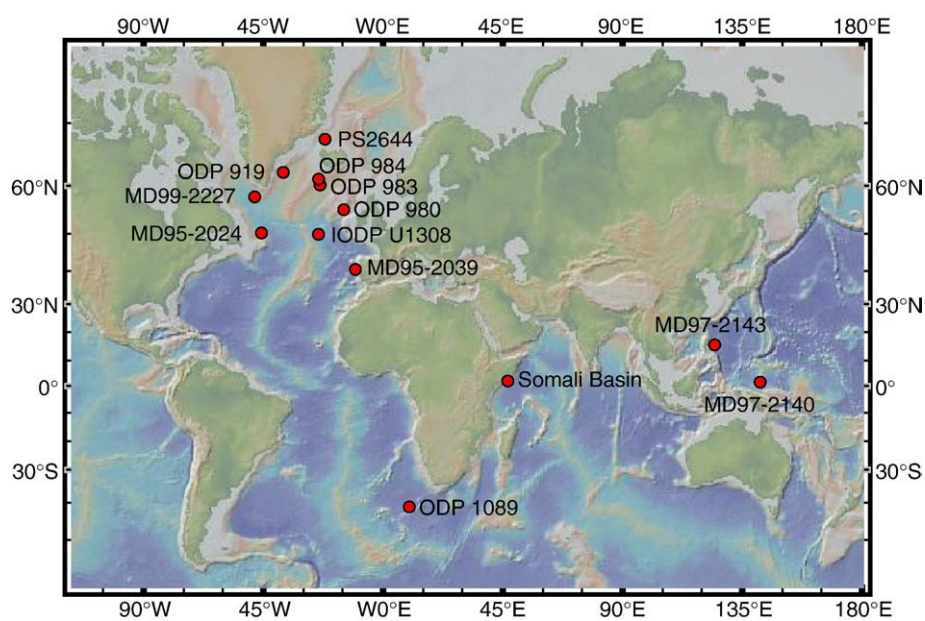

Fig. 1. Location of the 13 coupled isotope and relative paleointensity records used in this analysis (see Table 1).

(Evans et al., 2007) extends back to 430 ka, and MD95-2039 (Thouveny et al., 2004; Thomson et al., 1999) extends back to 317 ka. The coupled isotope/RPI record from Core MD97-2140 covers the 560–1300 ka interval (Carcaillet et al., 2003, 2004; De Garidel-Thoron et al., 2005). Three records that cover the last glacial cycle only: MD95-2024 (Stoner et al., 2000), the Somali Basin record (Meynadier et al., 1992), and PS2644 (Laj et al., 2000; Voelker et al., 1998) are included to strengthen the stack in this interval (Table 1).

The use of the Match protocol here differs from its use in a recent paper (Channell et al., 2008) where we applied the protocol to RPI records only, and forced compatibility with oxygen isotope records by inserting hard tie points (usually at terminations) derived from the marine isotope records. By applying the Match protocol to the RPI and isotope records in tandem, we make better use of the isotope record and provide an improved test of the compatibility of RPI and isotope records. Each RPI and isotope record (Table 1) is matched to the IODP Site U1308 records, after normalizing each RPI or isotope record to have zero mean and one standard deviation. The starting points for each match are the original (published) age models (references in Table 1). In the Match protocol, each RPI and isotope record is divided into time "intervals" (with initial ~1 kyr duration in our case), and each ~1 kyr "interval" is matched to "interval(s)" in the Site U1308 records. The quality of the fit of a particular "interval" to "interval(s)" at Site U1308 is gauged by the sum of the squares of the differences for the data points within each "interval" pair. The optimal correlation of the two records is determined by minimization of the squares of the differences through the dynamic programming procedure (Lisiecki and Lisiecki, 2002), with penalty functions limiting the likelihood of abrupt sedimentation rate changes both within an individual record and between record pairs. The data points from one "interval" may lie anywhere along the interpolated line connecting data points in the "interval" with which it is compared. The sequential order of data points within an "interval", and the order of "intervals" in each time series, must be maintained. When matching multiple data types (e.g. RPI and oxygen isotopes), the oxygen isotope data are linearly interpolated to the same age scale as the RPI records, and Match computes the sum of the squares of the differences for each data type to find the optimal match. Unlike routine eyeball signal correlations, the Match correlations are repeatable and unbiased, and less likely to be diverted by local solutions.

The quality of fit represented by the Match output (Fig. 2) is checked visually for obvious discrepancies, and then formally tested in two ways.

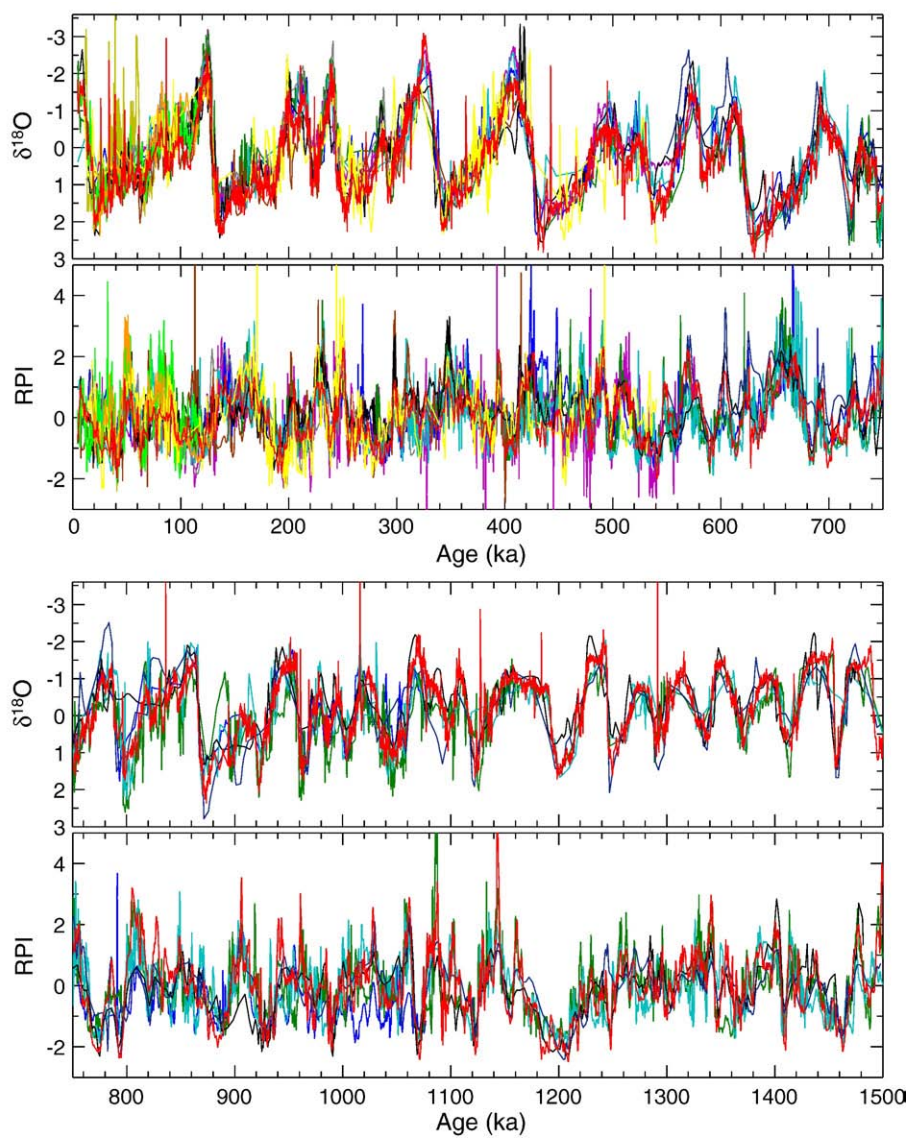

Fig. 2. Oxygen isotope and relative paleointensity (RPI) data from the 13 sites (color coded in Table 1) used to construct the RPI and isotope stacks, after optimal simultaneous matching of the RPI and isotopes to the Site U1308 records (in red).

Table 2
Correlation coefficient and percentage of significant area (at 5% level, on WTC maps) between IODP U1308 records (both paleointensity and oxygen isotope records) and other collected records before and after 'matching'.

		ODP 983	ODP 984	ODP 919	ODP 980	ODP 1089	MD97-2143	MD95-2024	MD95-2039	MD99-2227	PS 2644	Somali Basin	MD97-2140
Correlation coefficient	RPIs before 'matching'	0.2816	0.2728	0.2644	0.2255	0.4347	0.3272	0.3169	0.3512	0.2616	0.6432	0.4893	0.2553
	RPIs after 'matching'	0.7083	0.6742	0.6091	0.5661	0.7144	0.6891	0.5639	0.6141	0.6565	0.7592	0.6058	0.6676
	ISOs before 'matching'	0.6279	0.5597	0.4275	0.7068	0.8230	0.6908	0.7061	0.8502	0.7175	0.3732	0.7423	0.6431
	ISOs after 'matching'	0.8017	0.8091	0.6934	0.8537	0.8817	0.8277	0.8129	0.8726	0.8501	0.4724	0.7838	0.7558
Percentage of significant area	RPIs before 'matching'	0.4320	0.4739	0.3921	0.5078	0.5536	0.4630	0.4949	0.3680	0.4301	0.5857	0.5066	0.5588
	RPIs after 'matching'	0.7807	0.7193	0.6499	0.7086	0.7429	0.7204	0.5748	0.5634	0.7311	0.7869	0.5647	0.7321
	ISOs before 'matching'	0.6625	0.5824	0.5048	0.6503	0.7079	0.5775	0.5679	0.6872	0.5612	0.3805	0.2052	0.6599
	ISOs after 'matching'	0.7092	0.6515	0.5906	0.7051	0.6938	0.6747	0.5461	0.7228	0.5616	0.4582	0.4707	0.6832

Firstly, the correlation coefficients between IODP Site U1308 records and the other records are calculated before and after matching RPI and isotope data (Table 2). RPI and isotope data from each record were interpolated to the age scale of IODP Site U1308 before calculation of correlation coefficients. The "before match" correlation coefficients correspond to the match of record pairs on their published age models (Table 1). Note that, in all cases, the correlation coefficients are increased, often substantially, after matching (Table 2). Secondly, we test whether the matching process has indeed improved the correlation in time–frequency space by calculating the squared wavelet coherence (WTC) before and after matching. The definition of the WTC resembles that of a traditional correlation coefficient, and can be thought of as a localized correlation coefficient in time–frequency space. It can be used to identify both frequency bands and time intervals within which the two time series are co-varying and statistical significance levels can be determined using Monte Carlo methods (Torrence and Compo, 1998; Grinsted et al., 2004). The RPI and oxygen isotope data were linearly interpolated at 1-kyr increments prior to calculation of squared wavelet coherence (WTC). As an example, we plot the WTC before and after matching of RPI and isotope data for ODP Site 983 and IODP Site U1308 (Fig. 3). For both RPI and isotope data from these two sites, we observe an improvement in coherence of RPI and isotope records after matching (more area with significant WTC and constant phase relationship), compared to the original age models (Fig. 3). The improvement is evident in the 10–200 kyr period range, indicating lower record sensitivity for periods below 10 kyr. In Table 2, the improved correlation to IODP Site U1308 after matching is expressed as the percentage of significant (at 5% level) area on WTC maps (red area bounded by thick black line in Fig. 3) before and after matching. Data within the cone of influence (where edge effects make the analyses unreliable) were ignored when counting the significant areas. In all but one case, both correlation coefficients and percentages of significant WTC indicate that the Match protocol improves the fit of both RPI and isotope data to the Site U1308 records (Table 2). The one exception is the MD95-2024 (planktic) isotope record

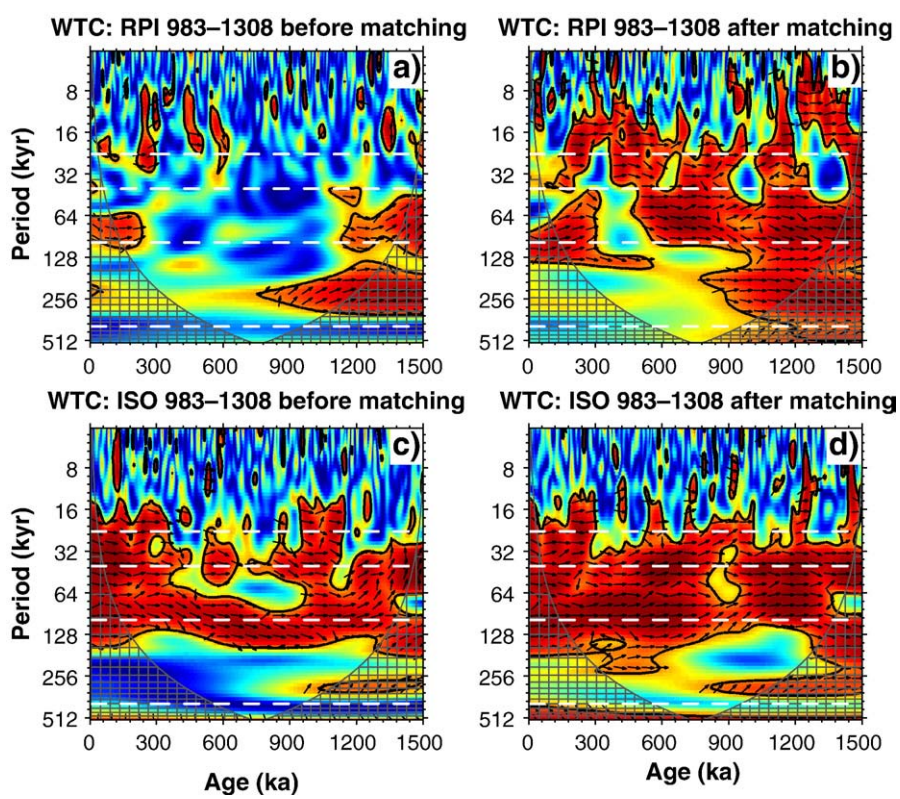

Fig. 3. Squared wavelet coherence (WTC) between the relative paleointensity (RPI) records from ODP Site 983 and IODP Site U1308 before and after simultaneous matching using the Match protocol. Values of squared wavelet coherence are indicated using different colors (with blue to red indicating increasing values). The 5% significance level against red noise is shown as thick contours. The cones of influence (COI) where edge effects make the analyses unreliable are marked by areas of crossed lines. The relative phase relationship is shown as arrows (with in-phase pointing right, anti-phase pointing left, and first signal leading second by 90° pointing down). Orbital periods of 404 kyr, 100 kyr, 41 kyr, and 23 kyr are marked by white dashed lines.

where although the correlation coefficients indicate improvement of fit after matching, the percentage of significant WTC indicates no significant improvement for the isotope records (Table 2).

The stack is constructed for RPI and oxygen isotopes by re-sampling each matched RPI and isotope record, and the reference records from IODP Site U1308, at 1-kyr sample spacing. The arithmetic mean, determined at each point, constitutes the stacked record (Fig. 4). The standard error (σ) is determined by (bootstrap) calculations from 1 million random samplings of data points associated with each point in the stack. The half-width of the error envelope in Fig. 4 equals 2σ. The PISO-1500 stacks can be found in Supplementary Data as two files.

3. Comparison with other stacks

The ~100 kyr-scale features in the new stack are largely compatible with the Sint-2000 stack (Valet et al., 2005) (Fig. 4) and enhanced detail in the new stack can be attributed to higher sedimentation rate records included in the new stack as well as the use of coupled isotope/RPI matching that reduces age discrepancies among the stacked records. The Sint-2000 stack is an extension of the earlier Sint-800 (Guyodo and Valet, 1999), and comprises records from the world's oceans including the ODP Leg 138 record and the younger parts of ODP Sites 983 and 984. The resolution of the Sint-2000 stack is limited by low sedimentation rates and poor age control for some of the records, and smoothing inherent in the stacking process. In Fig. 5, we compare the new stack with the EPAPIS Pacific stack (Yamazaki and Oda, 2005), the equatorial Pacific record from ODP Leg 138 (Valet and Meynadier, 1993) and the record of paleointensity derived from the East Pacific Rise (EPR) magnetic anomaly data (Gee et al., 2000). Whereas the age calibration of the EPR record is loosely constrained by spreading rate assumptions, the ODP Leg 138 record is rather precisely calibrated by astrochronology (Shackleton et al., 1995) although low mean sedimentation rates (1–2 cm/kyr) limit the resolution of the record. Mean sedimentation rates in the EPAPIS Pacific stack are also <2 cm/kyr (Yamazaki and Oda, 2005). The EPAPIS age model relies on the correlation of lows in magnetic concentration parameters (susceptibility and anhysteretic remanence intensity) with glacial intervals in a reference oxygen isotope record, in effect relying on the "Indo-Pacific"

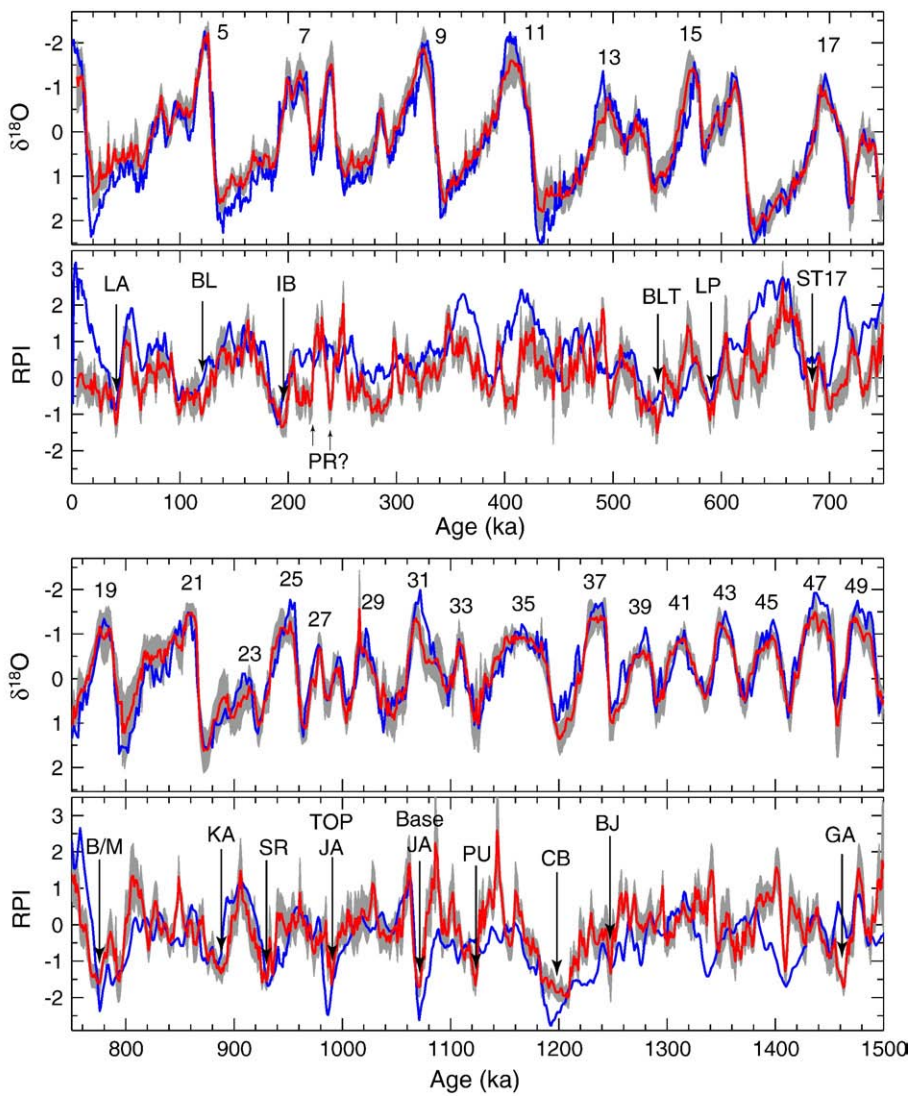

Fig. 4. Oxygen isotope and relative paleointensity (RPI) stacks (both in red) based on data in Fig. 2. Half-width of the error envelope in both cases is 2σ ($2\times$standard error) computed using the bootstrap method for 1 million samplings. The oxygen isotope stack (red) is compared with the LR04 benthic isotope stack (blue) (Lisiecki and Raymo, 2005), and the RPI stack (red) is compared with Sint-2000 stack (blue) (Valet et al., 2005). In this plot, the Sint-2000 data have been subtracted from their mean and divided by their standard deviation. Paleointensity minima in the stack correspond to established ages of magnetic excursions and chron/subchron boundaries: LA-Laschamp, BL—Blake, IB—Iceland Basin, PR—Pringle Falls, BLT—Big Lost, LP—La Palma, ST17—Stage 17, B/M—Brunhes–Matuyama boundary, KA—Kamikatsura, SR—Santa Rosa, JA—Jaramillo Subchron, PU—Punaruu, CB—Cobb Mt. Subchron, BJ—Bjorn, GA—Gardar. (For interpretation of the references to color in this figure legend, the reader is referred to the web version of this article.)

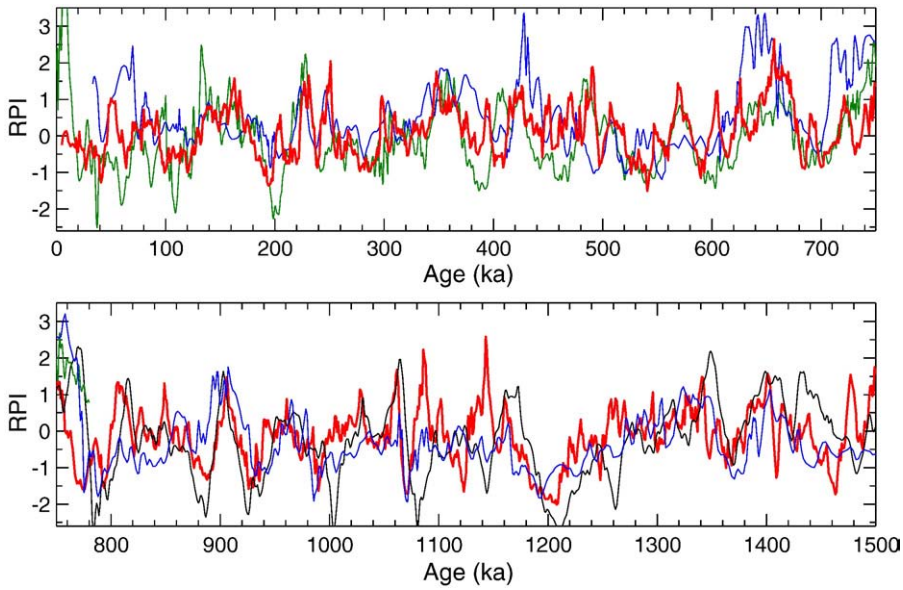

Fig. 5. The new paleointensity stack (PISO-1500, red) compared with the EPAPIS Pacific stack (black) (Yamazaki and Oda, 2005), with the inversion of magnetic anomaly data from the East Pacific Rise (green) (Gee et al., 2000) and the RPI record from ODP Leg 138 (blue) (Valet and Meynadier, 1993). In this plot, these records have been subtracted from their means and divided by their standard deviations. (For interpretation of the references to color in this figure legend, the reader is referred to the web version of this article.)

carbonate pattern of high carbonate content during glacial intervals. Interestingly, the age of features in the EPAPIS stack appear to be displaced to older ages relative to correlative features in the PISO-1500 stack (Fig. 5), implying an offset in carbonate (and magnetic) concentration and isotope stages in the EPAPIS cores. This type of offset, resulting from carbonate concentration variations lagging benthic δ^{18}O, has been documented in the "Indo-Pacific" carbonate pattern of the sub-Antarctic South Atlantic (Hodell et al., 2001).

4. Discussion

Benthic δ^{18}O stratigraphy has been the gold standard for correlation of Quaternary marine sequences, but this tool has important limitations, especially for shorter timescales (Skinner and Shackleton, 2005, 2006). Simultaneous matching of isotope and RPI signals (from the same cores) provides additional constraints on oxygen isotope correlations and may allow detection of subtle leads and lags among aspects of the climate system. Simultaneous correlation of RPI and isotope records reduces the degree of freedom associated with correlations using RPI or isotope records alone, and serves as a test for the consistency of RPI and isotope correlations. The PISO-1500 RPI stack is based on 13 coupled RPI/isotope records where record matching is accomplished by simultaneous optimization of RPI/isotope records using the Match protocol (Lisiecki and Lisiecki, 2002).

The fidelity of the PISO-1500 isotope stack can be gauged by comparison with the LR04 isotope stack (Lisiecki and Raymo, 2005) (Fig. 4). Local wavelet power spectra (LWPS) for the PISO-1500 isotope stack (Fig. 6d) and LR04 (Fig. 6b) indicate very similar distributions of significant orbital power in the two stacks, implying that the resolution of the two stacks is comparable. Note that the mid-Pleistocene climate transition from 41 kyr to 100 kyr power, at about 800 ka, is well represented in LWPS maps of both the LR04 and PISO-1500 isotope stacks (Fig. 6b and d).

Non-axial-dipole (NAD) components in the historical field vary on centennial timescales (Hulot and Le Mouël, 1994; Hongre et al., 1998; Valet et al., 2008) and if similar repeat times hold in the geologic past, paleointensity records from cores with sedimentation rates less than ~15 cm/kyr are unlikely to record anything but the axial dipole field, and therefore should represent a global signal.

In the last 10 yr, there has been considerable debate over the observation and interpretation of orbital periods in RPI data (Channell et al., 1998; Yamazaki, 1999; Yokoyama and Yamazaki, 2000; Guyodo et al., 2000; Yamazaki and Oda, 2002; Roberts et al., 2003; Yokoyama et al., 2007; Thouveny et al., 2008; Xuan and Channell, 2008a,b). Some authors considered that the orbital power in RPI records can be attributed to the geodynamo (e.g. Yokoyama et al., 2007) while others considered that it is due to lithologic/climatic "contamination" of some RPI records (e.g. Xuan and Channell, 2008b).

Although there are patches of significant power at orbital periods in the PISO-1500 RPI stack (Fig. 6c) and Sint-2000 (Fig. 6a), there is much less significant orbital power in the stacks than in some RPI individual records (see Xuan and Channell, 2008b). The distribution of significant power in these plots (Fig. 6a and c) is dependent on the estimated level of (AR1) noise, which is set at 0.9264 for both stacks (estimated using the PISO-1500 RPI stack). The squared wavelet coherence map (Fig. 6e) indicates significant coherence between the PISO-1500 RPI and isotope stacks during limited time intervals (e.g. 660–810 ka and 1120–1240 ka) and in variable frequency bands. The phase relationships between the two records, however, vary during these time intervals (see Fig. 6e) implying either a non-linear relationship between the two records or, more probably, a fortuitous occurrence of significant coherence of two unrelated records that have power in similar frequency bands. A visual comparison between the PISO-1500 RPI and δ^{18}O stacks shows positive correlations at ~660–810 ka (shaded area in Supplementary Fig. 1) and negative correlations at ~1120–1240 ka (shaded area in Supplementary Fig. 1), consistent with the WTC map (Fig. 6e). The patch of significant orbital power (at ~90 kyr) at ~600–800 ka in the PISO-1500 RPI stack (Fig. 6c) appears significantly coherent with the isotope stack (Fig. 6e), implying (climate-related lithological) contamination in this part of the RPI stack.

The inventory of magnetic excursions (brief quasi polarity chrons with duration less than ~10 kyr) has developed over the last 20 yr to the point where about 7 magnetic excursions are reasonably well documented in the Brunhes Chron, with about the same number having been adequately recorded in the later part of the Matuyama Chron (see Laj and Channell, 2007). The brief (< few kyr) duration of directional excursions makes their observation problematic even for sediments with mean sedimentation rates above 10 cm/kyr because of smoothing (filtering of higher frequency remanence variations) associated with the

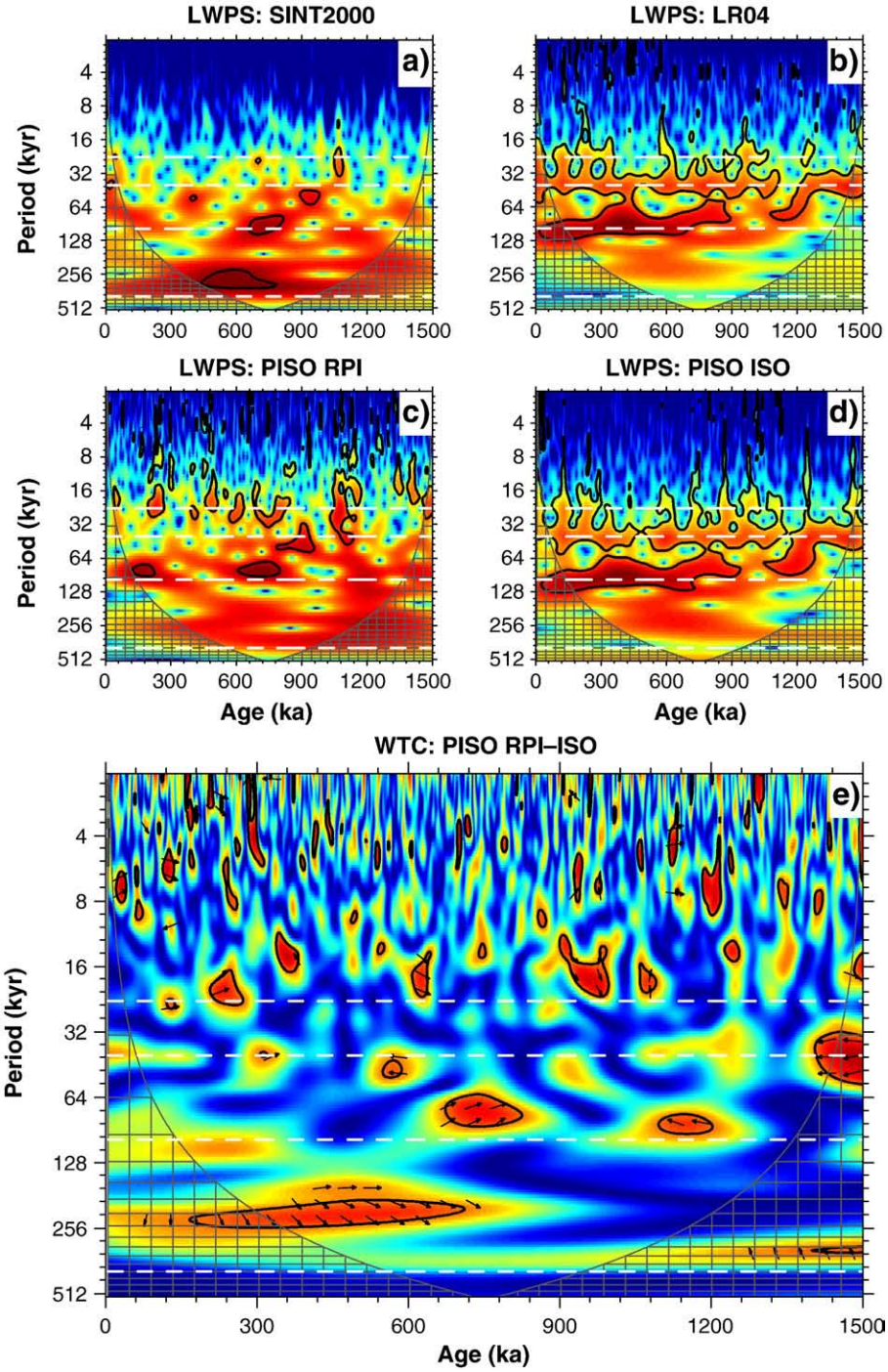

Fig. 6. Local wavelet power spectrum (LWPS) of: (a) the Sint-2000 relative paleointensity (RPI) stack (Valet et al., 2005), (b) the LR04 benthic oxygen isotope stack of Lisiecki and Raymo (2005), (c) the new PISO-1500 RPI stack and (d) the PISO-1500 oxygen isotope stack, and (e) squared wavelet coherence (WTC) between the PISO-1500 RPI and oxygen isotope stacks. Values of normalized wavelet power and squared wavelet coherence are indicated using different colors on LWPS and WTC maps (with blue to red indicating increasing values). The 5% significance level against red noise is shown as thick contours in all figures. The cones of influence (COI) where edge effects make the analyses unreliable are marked by areas of crossed lines. In (e), the relative phase relationship is shown as arrows (with in-phase pointing right, anti-phase pointing left, and first signal leading second by 90° pointing down. Orbital periods of 404 kyr, 100 kyr, 41 kyr, and 23 kyr are marked by white dashed lines.

remanence acquisition, the stochastic (non-uniform) nature of sediment deposition, and the effects of bioturbation. The paleointensity lows associated with magnetic excursions (and polarity reversals), on the other hand, have greater duration than the associated directional excursions and are often clearly observed in individual RPI records, even when the directional excursion is not. In the PISO-1500 RPI stack, the ages of excursions coincide with paleointensity minima in the stack (Fig. 4).

In order to calibrate the new RPI stack and arrive at temporal variations in virtual axial dipole moment (VADM), we adopted the value of 7.46×10^{22} Am^2 for the time averaged VADM for the last 800 kyr from Valet et al. (2005), based on an analysis of the volcanic paleointensity (PINT03) database of Perrin and Schnepp (2004). We then scaled the stack to this mean value (for the last 800 kyr) and assigned an intensity of 7.5 μT at IODP Site U1308 (the reference record) for the minimum RPI value in the stack, that lies within the Cobb Mountain Subchron (Fig. 4).

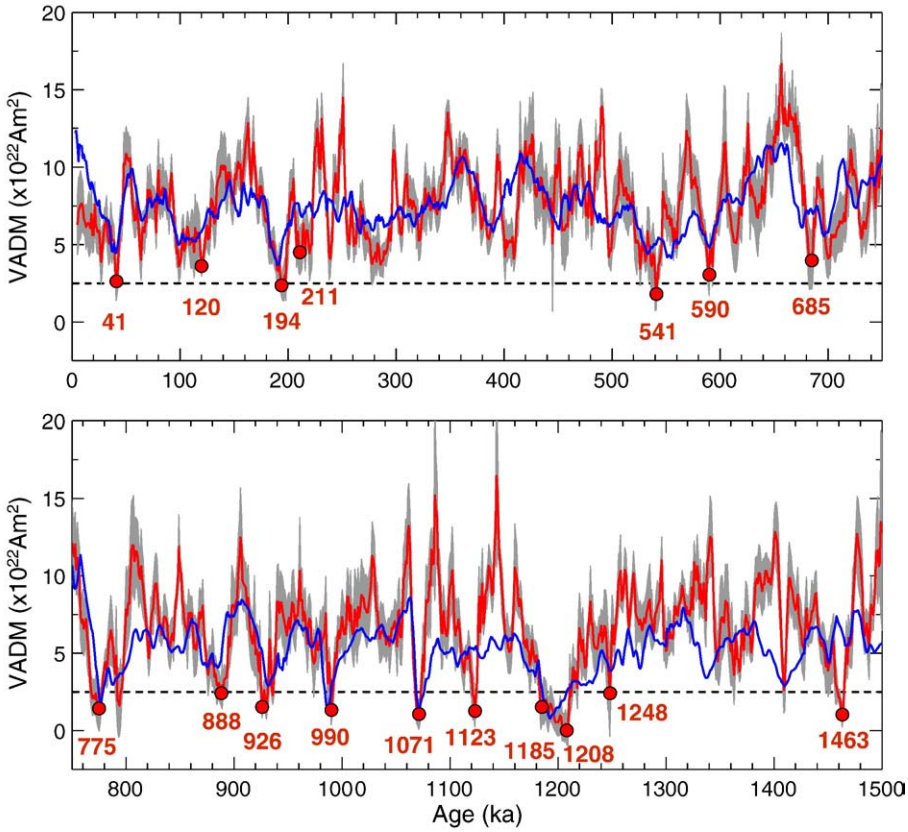

Fig. 7. Virtual axial dipole moment (VADM) calibration of the PISO-1500 relative paleointensity stack (red). See text for calibration procedure. Half-width of the error envelope is 2σ ($2\times$standard error) computed using the bootstrap method for 1 million samplings. The VADM values for the Sint-2000 stack (Valet et al., 2005) are in blue. Red dots indicate paleointensity minima that have ages close to those attributed to geomagnetic excursions and reversals (see Fig. 4 for excursion/reversal labels). The dashed line represents the threshold value of 2.5×10^{22} Am^2 that appears to trigger excursions and reversals. (For interpretation of the references to color in this figure legend, the reader is referred to the web version of this article.)

This procedure follows Constable and Tauxe (1996) who suggested scaling RPI records by using this minimum intensity value, based on the modern field, that corresponds to the likely value of the residual field after total demise of the axial dipole (at times of reversal). The resulting scaling (Fig. 7) yields a VADM value appropriate for the recent field (~7.5×10^{22} Am^2), maxima of ~15×10^{22} Am^2 at ~660 ka and between the Jaramillo and the Cobb Mountain subchrons, and an apparent threshold VADM value of ~2.5×10^{22} Am^2 associated with excursions and reversals. Comparison of Figs. 4 and 7 indicates that almost all VADM values below this threshold are associated with either excursions or reversals. Note that the Cobb Mountain Subchron (at ~1200 ka) appears as an exceptionally long interval (~30 kyr) of particularly low field intensity. The VADM values for the last 1.5 Myr do not show an increase in paleointensity at the onset of the Brunhes Chron analogous to that seen in Sint-2000 (see Fig. 2a in Valet et al., 2005). The mean VADM is higher for the Brunhes Chron (7.5×10^{22} Am^2) than for the late Matuyama (6.8×10^{22} Am^2); however, this difference in mean VADM is less than the mean value of the standard error associated with the stack (0.77), and therefore the two mean values are not statistically distinguishable. Note that the mean Brunhes VADM is close to the apparent modern field value, which is close to its actual modern value although this value is not set as part of the scaling process. The range of VADM values associated with PISO-1500, reaching more than 15×10^{22} Am^2 (Fig. 7), is consistent with the range of values for the last few million years in the volcanic PINT06 database (see Fig. 18 in Tauxe and Yamazaki, 2007).

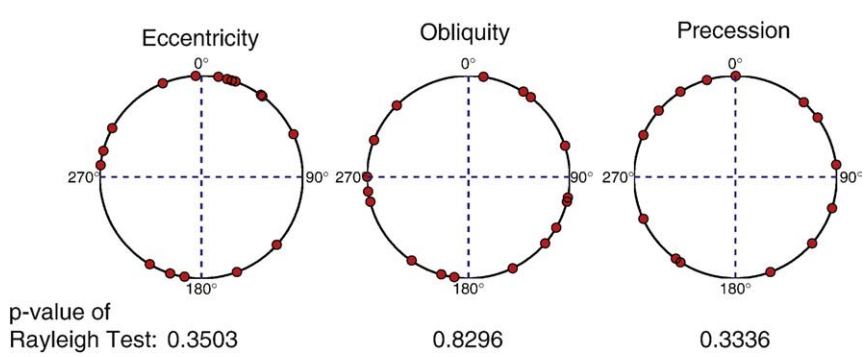

Fig. 8. Circular plot of phase of orbital eccentricity, obliquity and precession (Laskar et al., 2004) corresponding to 17 relative paleointensity (RPI) lows labeled in Fig. 7. The *p*-values associated with the Rayleigh Test are indicated for each distribution (see Xuan and Channell, 2008a, for further details).

Following Fuller (2006), Thouveny et al. (2008) have made the case for a link between RPI and orbital obliquity in which RPI lows are associated with a particular phase (minima or decreasing obliquity angles) in the obliquity cycle. This relationship has been thought to be due to common orbital forcing for RPI and oxygen isotope values (Thouveny et al., 2008). Although there is no statistical evidence for a relationship between the obliquity angle and ages of excursions and reversals on longer timescales (Xuan and Channell, 2008a), the new stack provides us with the opportunity to test the relationship between the obliquity angle (and other orbital cycles) and RPI. Following the methods described by Xuan and Channell (2008a), and assuming no uncertainty in the ages of the RPI minima or in the astronomical solution, we compute the phases, as defined by Xuan and Channell (2008a), of the orbital eccentricity, obliquity, and precession at the time of the prominent RPI minima (as labeled in Fig. 7). The results are shown in Fig. 8 with *p*-values associated with the Rayleigh test, indicating that we cannot reject a circular uniform distribution of RPI minima relative to the phases of any of the orbital parameters (even at a 30% significance level). In other words, there is no tendency for RPI minima in the stack to occur at particular phases of orbital variations such as lows or decreasing values of obliquity. Visually, the timing of the prominent RPI lows in the stack (red dots in Supplementary Fig. 1) do not appear to preferentially occur at obliquity lows or in the decreasing part of the obliquity cycles.

5. Conclusions

The PISO-1500 RPI stack provides a template for geomagnetic paleointensity for the last 1.5 Myr. The stack has higher temporal resolution than earlier stacks such as Sint-2000 (Valet et al., 2005) due to the addition of new RPI/isotope records and the use of coupled isotope and RPI records that allow the simultaneous correlation of isotope and RPI records using the Match algorithm (Lisiecki and Lisiecki, 2002). The advantage of this procedure is that it limits the degree of freedom associated with individual signal correlations, is repeatable, and allows assessment of the compatibility of RPI and isotope records. The tandem stacks provide a powerful stratigraphic tool that can be used to correlate among marine sediment records, and link them to polar ice cores via cosmogenic nuclide flux. RPI data from marine cores have been correlated to modelled paleointensity based on cosmogenic nuclide flux in Greenland ice cores (e.g. Muscheler et al., 2005), and to $^{10}Be/^{9}Be$ data derived from the sediments themselves (e.g. Carcaillet et al., 2004). Once a continuous record of comogenic isotope abundance has been completed for the 800-kyr record from EPICA-Dome C (Jouzel et al., 2007), correlation to the new PISO-1500 stack will permit synchronization of marine and ice cores. This will eventually allow transfer of ice core chronologies, such as those derived by correlation of N_2/O_2 to local insolation forcing (Kawamura et al., 2007), to the marine record (and vice-versa). Such an independent marine chronology could eventually eliminate difficulties inherent in oxygen isotope stratigraphy such as the assignment of phase lag between forcing and response implicit in insolation-driven ice-sheet models (Imbrie and Imbrie, 1980), and the assumption that $\delta^{18}O$ is purely a glacial ice volume signal. In the future, the timing and phase relationships of components of the climate system may be resolvable independent of oxygen isotope stratigraphy, thereby advancing our understanding of the mechanisms of glacial–interglacial climate change.

Acknowledgements

We thank C.-S. Horng, N. Thouveny, J-P. Valet, J. Stoner and C. Laj for supplying data. N. Thouveny and L.E. Lisiecki provided helpful reviews of an earlier version of the manuscript. Wavelet analyses were performed using modified versions of MATLAB codes originally written by C. Torrence and G. Compo, and by A. Grinsted.

Appendix A. Supplementary data

Supplementary data including the PISO-1500 paleointensity and isotope stacks can be found, in the online version, at doi:10.1016/j.epsl.2009.03.012.

References

Carcaillet, J.T., Thouveny, N., Bourles, D.L., 2003. Geomagnetic moment instability between 0.6 and 1.3 Ma from cosmonuclide evidence. Geophys. Res. Lett., 30 (15), 1792. doi:10.1029/2003GL017550.

Carcaillet, J.T., Bourles, D.L., Thouveny, N., 2004. Geomagnetic dipole moment and ^{10}Be production rate intercalibration from authigenic $^{10}Be/^{9}Be$ for the last 1.3 Ma. Geochem. Geophys. Geosysyt. 5 (5), Q05006. doi:10.1029/2003GC000641.

Channell, J.E.T., 1999. Geomagnetic paleointensity and directional secular variation at Ocean Drilling Program (ODP) Site 984 (Bjorn Drift) since 500 ka: comparisons with ODP Site 983 (Gardar Drift). J. Geophys. Res. 104, 22,937–22,951.

Channell, J.E.T., 2006. Late Brunhes polarity excursions (Mono Lake, Laschamp, Iceland Basin and Pringle Falls) recorded at ODP Site 919 (Irminger Basin). Earth Planet. Sci. Lett. 244, 378–393.

Channell, J.E.T., Kleiven, H.F., 2000. Geomagnetic palaeointensities and astrochronological ages for the Matuyama–Brunhes boundary and the boundaries of the Jaramillo Subchron: palaeomagnetic and oxygen isotope records from ODP Site 983. Philos. Trans. R. Soc. Lond. A 358, 1027–1047.

Channell, J.E.T., Raymo, M.E., 2003. Paleomagnetic record at ODP Site 980 (Feni Drift, Rockall) for the past 1.2 Myrs. Geochem. Geophys. Geosyst. 4, 1033. doi:10.1029/2002GC000440.

Channell, J.E.T., Hodell, D.A., Lehman, B., 1997. Relative geomagnetic paleointensity and $\delta^{18}O$ at ODP Site 983 (Gardar Drift, North Atlantic) since 350 ka. Earth Planet. Sci. Lett. 153, 103–118.

Channell, J.E.T., Hodell, D.A., McManus, J., Lehman, B., 1998. Orbital modulation of the Earth's magnetic field intensity. Nature 394, 464–468.

Channell, J.E.T., Mazaud, A., Sullivan, P., Turner, S., Raymo, M.E., 2002. Geomagnetic excursions and paleointensities in the Matuyama Chron at Ocean Drilling Program Sites 983 and 984 (Iceland Basin). J. Geophys. Res. 107, 2114. doi:10.1029/2001JB000491.

Channell, J.E.T., Hodell, D.A., Xuan, C., Mazaud, A., Stoner, J.S., 2008. Age calibrated relative paleointensity for the last 1.5 Myr at IODP Site U1308 (North Atlantic). Earth Planet. Sci. Lett. 274, 59–71.

Constable, C., Tauxe, L., 1996. Towards absolute calibration of sedimentary paleointensity records. Earth Planet. Sci. Lett. 143, 269–274.

De Garidel-Thoron, T., Rosenthal, Y., Bassinot, F., Beaufort, L., 2005. Stable sea surface temperatures in the western Pacific warm pool over the past 1.75 million years. Nature 433, 294–298.

Evans, H.F., Channell, J.E.T., Stoner, J.S., Hillaire-Marcel, C., Wright, J.D., Neitzke, L.C., Mountain, G.S., 2007. Paleointensity-assisted chronostratigraphy of detrital layers on the Eirik Drift (North Atlantic) since marine isotope stage 11. Geochem. Geophys. Geosyst. 8 (11). doi:10.1029/2007GC111720.

Fuller, M., 2006. Geomagnetic field intensity, excursions, reversals and the 41,000-yr obliquity signal. Earth Planet. Sci. Lett. 245, 605–615.

Gee, J.S., Cande, S.C., Hildebrand, J.A., Donnelly, K., Parker, R.L., 2000. Geomagnetic intensity variations over the past 780 kyr obtained from near-seafloor magnetic anomalies. Nature 408, 827–832.

Grinsted, A., Moore, J.C., Jevrejeva, S., 2004. Application of the cross wavelet transform and wavelet coherence to geophysical time series. Nonlin. Processes. Geophys. 11, 561–566.

Guyodo, Y., Valet, J.P., 1999. Global changes in intensity in the Earth's magnetic field during the past 800 kyr. Nature 399, 249–252.

Guyodo, Y., Gaillot, P., Channell, J.E.T., 2000. Wavelet analysis of relative geomagnetic paleointensity at ODP Site 983. Earth Planet. Sci. Lett. 184, 109–123.

Hodell, D.A., Charles, C.D., Sierro, F.J., 2001. Late Pleistocene evolution of the ocean's carbonate system. Earth Planet. Sci. Lett. 192, 109–124.

Hodell, D.A., Channell, J.E.T., Curtis, J.H., Romero, O.E., Rohl, U., 2008. Onset of "Hudson Strait" Heinrich Events in the eastern North Atlantic at the end of the Middle Pleistocene Transition (~640 ka)? Paleoceanography 23, PA4218. doi:10.1029/2008PA001591.

Hongre, L., Hulot, G., Khokhlov, A., 1998. An Analysis of the geomagnetic field over the past 2000 years, Phys. Earth Planet. Int. 106, 311–335.

Horng, C.S., Roberts, A.P., Liang, W.T., 2003. A 2.14-Myr astronomically tuned record of relative geomagnetic paleointensity from the western Philippine Sea. J. Geophys. Res. 108, 2059. doi:10.1029/2001JB001698.

Horng, C.S., Lee, M.Y., Palike, H., Wei, K.Y., Liang, W.T., 2002. Astronomically calibrated ages for geomagnetic reversals within the Matuyama chron. Earth Planets Space 54, 679–690.

Hulot, G., Le Mouël, J.L., 1994. A statistical approach to the Earth's main magnetic field. Phys. Earth Planet. Int. 82, 167–183.

Imbrie, J., Imbrie, J.Z., 1980. Modeling the climatic response to orbital variations. Science 207, 943–953.

Jouzel, J., Masson-Delmotte, V., Cattani, O., Dreyfus, G., Falourd, S., Hoffmann, G., Minster, B., Nouet, J., Barnola, J.M., Chappellaz, J., Fischer, H., Gallet, J.C., Johnsen, S., Leuenberger, M., Loulergue, L., Luethi, D., Oerter, H., Parrenin, F., Raisbeck, G., Raynaud, D., Schilt, A., Schwander, J., Selmo, E., Souchez, R., Spahni, R., Stauffer, B., Steffensen, J.P., Stenni, B., Stocker, T.F., Tison, J.L., Werner, M., Wolff, E.W., 2007. Orbital and millennial Antarctic climate variability over the past 800,000 years. Science 317, 793–797.

Kawamura, K., Parrenin, F., Lisiecki, L., Uemura, R., Vimeux, F., Severinghaus, J.P., Hutterli, M.A., Nakazawa, T., Aoki, S., Jouzel, J., Raymo, M.E., Matsumoto, K., Nakata, H., Motoyama, H., Fujita, S., Goto-Azuma, K., Fujii, Y., Watanabe, O., 2007. Northern Hemisphere forcing of climatic cycles in Antarctica over the past 360,000 years. Nature 448, 912–916.

Korte, M., Constable, C., 2005. The geomagnetic dipole moment over the last 7000 years — new results from a global model. Earth Planet. Sci. Lett. 236, 348–358.

Laj, C., Channell, J.E.T., 2007. Geomagnetic excursions. In: Kono, M. (Ed.), Treatise on Geophysics: Volume 5, Geomagnetism. Elsevier, Amsterdam, pp. 373–416. Chapter 10.

Laj, C., Kissel, C., Mazaud, A., Channell, J.E.T., Beer, J., 2000. North Atlantic palaeointensity stack since 75 ka (NAPIS-75) and the duration of the Laschamp event. Philos. Trans. R. Soc. Lond. A 358, 1009–1025.

Laj, C., Kissel, C., Beer, J., 2004. High resolution global paleointensity stack since 75 kyr (GLOPIS-75) calibrated to absolute values. In: Channell, J.E.T., Kent, D.V., Lowrie, W., Meert, J.G. (Eds.), Timescales of the Paleomagnetic Field. Geophysical Monograph, vol. 145. Amercian Geophysical Union, Washington, DC, USA.

Laskar, J., Robutel, P., Joutel, F., Gastineau, M., Correia, A., Levrard, B., 2004. A long term numerical solution for the insolation quantities of the Earth. Astron. Astrophys. 428, 261–285.

Lisiecki, L.E., Lisiecki, P.A., 2002. Application of dynamic programming to the correlation of paleoclimate records. Paleoceanography 17, 1049. doi:10.1029/2001PA000733.

Lisiecki, L.E., Raymo, M.E., 2005. A Pliocene–Pleistocene stack of 57 globally distributed benthic d^{18}O records. Paleoceanography 20, PA1003. doi:10.1029/2004PA001071.

Meynadier, L., Valet, J.P., Weeks, R.J., Shackleton, N.J., Hagee, V.L., 1992. Relative geomagnetic intensity of the field during the last 140 ka. Earth Planet. Sci. Lett. 114, 39–57.

Muscheler, R., Beer, J., Kublik, P.W., Synal, H.A., 2005. Geomagnetic field intensity during the last 60,000 years based on ^{10}Be and ^{36}Cl from the Summit ice cores and ^{14}C. Quat. Sci. Revs. 24, 1849–1860.

Perrin, M., Schnepp, E., 2004. IAGA paleointensity database: distribution and quality of the dataset. Phys. Earth Planet. Int. 147, 255–267.

Roberts, A.P., Winklhofer, M., Liang, W.T., Horng, C.S., 2003. Testing the hypothesis of orbital (eccentricity) influence on Earth's magnetic field. Earth Planet. Sci. Lett. 216, 187–192.

Shackleton, N.J., 1967. Oxygen isotope analyses and Pleistocene temperature reassessed. Nature 215, 15–17.

Shackleton, N.J., Crowhurst, S., Hagelberg, T., Pisias, N.G., Schneider, D.A., 1995. A new Late Neogene time scale: application to Leg 138 Sites. In: Pisias, N.G., Janacek, L.A., Palmer-Julson, A., Van Andel, T.H. (Eds.), Proc. ODP Sci. Results, vol. 138, pp. 73–101.

Skinner, L.C., Shackleton, N.J., 2005. An Atlantic lead over Pacific deep-water change across Termination I: implications for the application of the marine isotope stage stratigraphy. Quat. Sci. Revs. 24, 571–580.

Skinner, L.C., Shackleton, N.J., 2006. Deconstructing Terminations I and II: revisiting the glacioeustatic paradigm based on deep-water temperature estimates. Quat. Sci. Rev. 25, 3312–3321.

Stoner, J.S., Channell, J.E.T., Hillaire-Marcel, C., Kissel, C., 2000. Geomagnetic paleointensity and environmental record from Labrador Sea Core MD95-2024: global marine sediment and ice core chronostratigraphy for the last 110 kyr. Earth Planet. Sci. Lett. 183, 161–177.

Stoner, J.S., Laj, C., Channell, J.E.T., Kissel, C., 2002. South Atlantic and North Atlantic geomagnetic paleointensity stacks (0–80 ka); implications for inter-hemispheric correlation. Quat. Sci. Rev. 21, 1141–1151.

Stoner, J.S., Channell, J.E.T., Hodell, D.A., Charles, C., 2003. A 580 kyr paleomagnetic record from the sub-Antarctic South Atlantic (ODP Site 1089). J. Geophys. Res. 108, 2244. doi:10.1029/2001JB001390.

Tauxe, L., Yamazaki, T., 2007. Paleointensities. In: Kono, M. (Ed.), Treatise on Geophysics. Geomagnetism, vol. 5. Elsevier, Amsterdam, pp. 509–563. Chapter 10.

Thomson, J., Nixon, S., Summerhayes, C.P., Schonfeld, J., Zahn, R., Grootes, P., 1999. Implications for sedimentation changes on the Iberian margin over the last two glacial/interglacial transitions from (^{230}Th excess) systematics. Earth Planet. Sci. Lett. 165, 255–270.

Thouveny, N., Carcaillet, J., Moreno, E., Leduc, G., Nerini, D., 2004. Geomagnetic moment variation and paleomagnetic excursions since 400 kyr BP; a stacked record from sedimentary sequences of the Portuguese margin. Earth Planet. Sci. Lett. 219, 377–396.

Thouveny, N., Bourles, D.L., Saracco, G., Carcaillet, J.T., Bassinot, F., 2008. Paleoclimatic context of geomagnetic dipole lows and excursions in the Brunhes, clue for an orbital influence on the geodynamo? Earth Planet. Sci. Lett. 275, 269–284.

Torrence, C., Compo, G.P., 1998. A practical guide to wavelet analysis. Bull. Am. Meteorol. Soc. 79, 61–78.

Valet, J.P., Meynadier, L., 1993. Geomagnetic field intensity and reversals during the past four million years. Nature 366, 234–238.

Valet, J.P., Meynadier, L., Guyodo, Y., 2005. Geomagnetic dipole strength and reversal rate over the past two million years. Nature 435, 802–805.

Valet, J.P., Herrero-Brevera, E., LeMouel, J.L., Plenier, G., 2008. Secular variation of the geomagnetic dipole during the past 2000 years. Geochem. Geophys. Geosyst. 9. doi:10.1029/2007GC001728.

Voelker, A.H.L., Sarnthein, M., Grootes, P.M., Erlenkeuser, H., Laj, C., Mazaud, A., Nadeau, M.J., Schleicher, M., 1998. Correlation of marine 14C ages from the Nordic Seas with GISP2 isotope record: implications for ^{14}C calibration beyond 25 ka BP. Radiocarbon 40, 517–534.

Xuan, C., Channell, J.E.T., 2008a. Testing the relationship between timing of geomagnetic reversals/excursions and phase of orbital cycles using circular statistics and Monte Carlo simulations. Earth Planet. Sci. Lett. 268, 245–254.

Xuan, C., Channell, J.E.T., 2008b. Origin of orbital periods in the sedimentary relative paleointensity records. Phys. Earth Planet. Inter. 169, 140–151.

Yamazaki, T., 1999. Relative paleointensity of the geomagnetic field during Brunhes Chron recorded in North Pacific deep-sea sediment cores: orbital influence? Earth Planet. Sci. Lett. 169, 23–35.

Yamazaki, T., Oda, H., 2002. Orbital influence on Earth's magnetic field; 100,000-year periodicity in inclination. Science 295, 2435–2438.

Yamazaki, T., Oda, H., 2005. A geomagnetic paleointensity stack between 0.8 and 3.0 Ma from Equatorial Pacific sediment cores. Geochem. Geophys. Geosyst. 6. doi:10.1029/2005GC001001.

Yokoyama, Y., Yamazaki, T., 2000. Geomagnetic paleointensity variation with a 100 kyr quasi-period. Earth Planet. Sci. Lett. 181, 7–14.

Yokoyama, Y., Yamazaki, T., Oda, H., 2007. Geomagnetic 100-kyr variation extracted from paleointensity records of the equatorial and north Pacific sediments. Earth Planets Space 59, 795–805.